A Magnetic Resonance Compatible Soft Wearable Robotic Glove for Hand Rehabilitation and Brain Imaging

Hong Kai Yap, *Student Member, IEEE*, Nazir Kamaldin, Jeong Hoon Lim, Fatima A. Nasrallah, James Cho Hong Goh, and Chen-Hua Yeow, *Member, IEEE*

***Abstract*— In this paper, we present the design, fabrication and evaluation of a soft wearable robotic glove, which can be used with functional Magnetic Resonance imaging (fMRI) during the hand rehabilitation and task specific training. The soft wearable robotic glove, called MR-Glove, consists of two major components: a) a set of soft pneumatic actuators and b) a glove. The soft pneumatic actuators, which are made of silicone elastomers, generate bending motion and actuate finger joints upon pressurization. The device is MR-compatible as it contains no ferromagnetic materials and operates pneumatically. Our results show that the device did not cause artifacts to fMRI images during hand rehabilitation and task-specific exercises. This study demonstrated the possibility of using fMRI and MR-compatible soft wearable robotic device to study brain activities and motor performances during hand rehabilitation, and to unravel the functional effects of rehabilitation robotics on brain stimulation.**

***Index Terms*— Magnetic resonance compatible devices, magnetic resonance compatible soft actuators, magnetic resonance imaging, rehabilitation robotics, soft wearable robotics.**

I. Introduction

HAND motor impairment is commonly observed in patients suffering from neurological disorders such as stroke. An individual's ability and independence to perform activities of daily living (ADLs) are compromised due to hand motor impairment. Patients with impaired hand function are required to undergo physical therapy, which involves repetitive task practice (RTP) rehabilitation that usually breaks down to specific tasks similar to those commonly performed in daily life such as grasping and pinching [1]. This is done to improve hand functions in terms of range of motion (ROM) and strength. In order to assist caregivers in the rehabilitation process and to provide a more quantitative assessment, robotic devices with the ability to carry out repetitive tasks have been proposed [2], [3].

While many clinical trials have been conducted to study the efficacy of various robot-assisted rehabilitation devices [4]–[6], the effectiveness of these interventions vary widely due to heterogeneity of mechanisms underlying motor recovery [7]. Recent development in neuroimaging techniques allows an in-depth investigation of brain motor recovery mechanisms. This is critical to better understanding the effectiveness of different rehabilitation techniques in treatment of neurological disorders [8], [9]. One of the most important neuroimaging techniques is functional magnetic resonance imaging (fMRI). fMRI has been widely used to investigate brain activity and reorganization in response to dynamic environments. Recent advances in neuroscience research using fMRI have gained a better understanding of brain neural plasticity and its relationship to motor recovery [10]. It gives important insights into brain mechanisms controlling voluntary movement as well as provides supporting evidence for optimal rehabilitation interventions and the development of rehabilitation robotics which can assist in the execution of motor tasks and study of brain responses using fMRI.

However, conducting fMRI studies with rehabilitation robotic devices faces a significant design challenge, which is the compatibility of devices with the magnetic resonance (MR) environment. Traditional robotic devices are normally made of rigid components such as linear actuators and rotary motors [11], [12]. These components usually contain ferromagnetic materials, which can interfere with the strong magnetic field in the MR environment. Hence, substantial forces may be generated under the magnetic field and cause safety concerns. Furthermore, conventional actuators and sensors potentially emit radio frequency energy that will distort the quality and introduce artifacts to the MR image [13]. For fMRI studies, the gradient echo-planar sequences are normally prone to interference from changes in the homogeneity of the static magnetic field due to the introduction and operation of electrical equipment inside the scanner bore or room [14]. Therefore, signal loss and distortion will occur and lead

Manuscript received June 1, 2015; revised November 19, 2015, July 7, 2016, and March 31, 2016; accepted August 22, 2016. Date of publication August 25, 2016; date of current version June 18, 2017. This work was supported by the Ministry of Education AcRF Tier 2 grant (R-397-000-203-112) and the NUHS–CIRC Seed Funding Grant (R-172-000-323-511). Corresponding author: Chen-Hua Yeow.

H. K. Yap and J. C. H. Goh are with the Department of Biomedical Engineering, National University of Singapore, Singapore 117583.

N. Kamaldin is with the Department of Electrical and Computer Engineering, National University of Singapore, Singapore 117583.

J. H. Lim is with the Department of Medicine, National University Hospital, Yong Loo Lin School of Medicine, National University of Singapore, Singapore 119228.

F. A. Nasrallah is with the Queensland Brain Institute, The University of Queensland, Brisbane, QLD 4072, Australia.

C.-H. Yeow is with the Department of Biomedical Engineering, National University of Singapore, Singapore 117583, and also with the Singapore Institute for Neurotechnology and Advanced Robotics Center (e-mail: bieych@nus.edu.sg).

Digital Object Identifier 10.1109/TNSRE.2016.2602941

to false activation or obscure true activation during fMRI studies.

Considering the limitations of traditional robotic devices under MR environment, a new design paradigm of actuators and sensors must be considered in order to build a MR-compatible robotic device. In the past few years, several MR-compatible robotic devices have been proposed for various applications such as prostate therapy, liver therapy, neurosurgery, MR steered drug delivery, rehabilitation, and haptic devices pertained to fMRI-based studies of brain activity [15]. Various actuation principles have also been proposed for robotic applications in MR environments [16]. For example, Riener *et al.* [17] proposed a haptic interface for a neuroscience application. The device consisted of a Lorentz motor that interacted with the large static magnetic field and produced a Lorentz force that mobilized the hand. However, the device suffered from low force output and its MR compatibility was dependent on its placement and orientation within the magnetic field [17].

Several MR-compatible force-sensing systems have also been proposed such as a hydraulic system that transmitted force to a pressure transducer outside of the scanner room [18], an ultrasonic motor with an optical force sensor based on reflected light intensity [19] and a MR-compatible load cell that measured isometric forces generated by the hand [20]. In a recent study, Khanicheh *et al.* proposed a device to study brain motor performances using fMRI during hand rehabilitation. The device utilized electrorheological fluids to generate force, and measured patient motion and applied force at the same time via an optical encoder and a force sensor [21]. However, the MR-compatible devices described above consisted largely of traditional rigid actuators and sensor components, which run the risk of causing damage or discomfort to the user during the MR experiment [22]. Additionally, it can be difficult to replicate perfectly the motion of natural joints with rigid devices, especially for human hands and fingers that possess high degrees of freedom (DOF).

Recently, new approaches have emerged with designs for hand robotic devices that are more wearable. These approaches utilize compliant materials such as cables or soft actuators for assisting hand and finger movements [23]–[29]. They are more portable and do not require complicated mechanical setups. This reduces setup time and the possibility of misalignment. Therefore, these devices are suitable for use as both rehabilitation and assistive devices that support task-specific training and simulated ADL tasks. Several research groups have developed soft hand robotic devices by combining wearable gloves with soft actuators [26]–[31]. For example, Connelly *et al.* have developed a pneumatic glove using inflatable air bladders that can assist finger extension [26]. Polygerinos *et al.* have designed a hydraulically actuated soft robotic glove that utilizes fiber-reinforced elastomeric actuators that can support finger motion [28]. One interesting characteristic of soft actuators is that they are made from non-ferromagnetic materials such as polyurethane and silicone elastomer. Thus, they are likely to remain functional in the MR environment and may not affect the MR environment. This feature motivated us to design a MR-compatible soft robotic glove, namely MR-Glove (Fig. 1), which can be used in fMRI studies in order to investigate the brain activity in relation to motor performance of the brain during simulated ADL tasks such as grasping and pinching.

Fig. 1. MR-Glove prototype.

Hence, the objective of this work was to develop and evaluate the MR-Glove that utilized pneumatically actuated soft elastomeric actuators, for use in task-specific training of hand movement in conjunction with fMRI. In Section II, we describe the soft actuator fabrication method and the design approach of the MR-Glove. Section III describes the quantitative and qualitative evaluation of the MR-Glove outside MR environment. Finally, in Section IV, we investigate the MR compatibility of the MR-Glove in a MR environment.

II. Design of a MR-Glove System for Applications in MR Environments

In this work, we aim to design a MR-Glove system that can be combined with fMRI to monitor the brain activation and to study the brain mechanisms and training-induced reorganization of the motor system during hand rehabilitation that emphasizes intense active movement repetition in performing simulated ADL tasks.

During the fMRI scans, the subject views a guidance video that displays the desired movement [Fig. 2(a)]. The MR-Glove can be programmed to operate in three modes:

(i) Passive movement mode, in which the subject's hand remains passive and the MR-Glove will provide assistance to guide the desired movement. This mode allows the study of whole brain response to passive movement kinematics involved in continuous passive motion [32].

(ii) Assistance-as-needed mode, in which the subject attempts to move and the MR-Glove supplements the effort [33]. A time-triggered assistive control strategy will be implemented [34]. The subject is provided 1–3 s to attempt the desired movement and the MR-Glove will then provide assistance for 1–3 s. If the subject fails to complete the hand movement with the desired range of motion, the MR-Glove

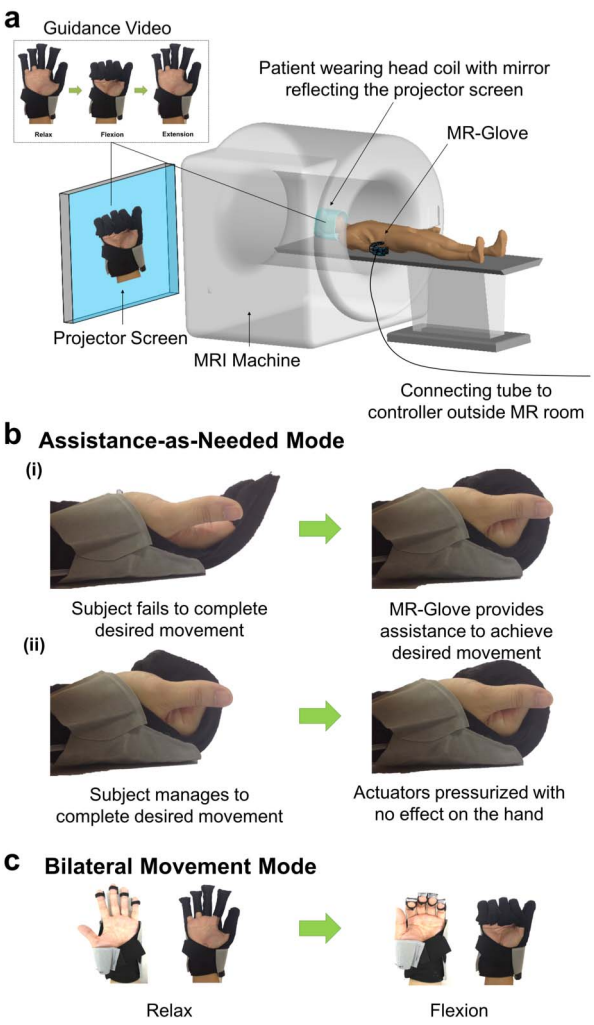

Fig. 2. (a) MR-Glove combined with fMRI. During the fMRI scans, the subject views a guidance video that displayed the desired movement. (b) Time-triggered Assistance-as-Needed Mode, (i) Subject is provided a certain time period to complete the desired movement. The MR-Glove provides assistance to complete the movement if the subject fails to complete the movement, (ii) If the subject manages to complete the desired movement, the actuators will be pressurized with no effect on the hand. (c) Bilateral Movement Mode. A MR-compatible data glove with ability to track the hand kinematics is worn on the nonparetic hand to detect the voluntary movements of the nonparetic hand and activate the MR-Glove on the paretic hand.

will move the hand to complete the range of motion. If the subject manages to complete the movement with the desired range of motion, the actuators of the MR-Glove will be simply pressurized with no effect on the hand [Fig. 2(b)]. As the glove utilizes flexible and low-impedance elastomeric actuators, it does not interfere with the hand movement when the subject attempts the desired movement. The time period given to the subject to attempt the movement can be adjusted based on the hand function, to be longer for subjects with poorer hand function and shorter for subjects with better hand function. This time-triggered assistive control strategy, combined with the guidance video, allows the subject to practice active repetitive movement by reconnecting intention to action [33].

(iii) Bilateral movement mode, in which the subject attempts to perform bimanual ADL tasks simultaneously.

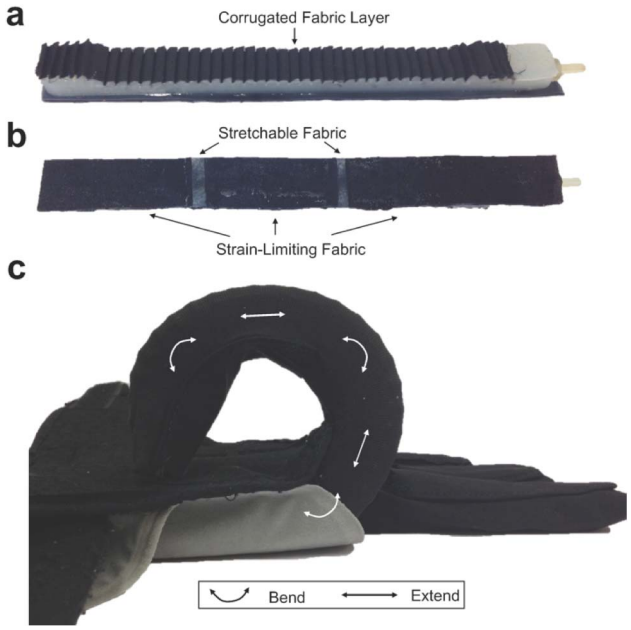

Fig. 3. (a) Side view of the actuator with corrugated-fabric layer. (b) Bottom view of the actuator with stretchable and strain-limiting fabrics. (c) Combination of motions achieved by the actuator inside the actuator pocket.

A MR-compatible data glove with ability to track the hand kinematics can be worn on the nonparetic hand in order to detect the voluntary movements of the nonparetic hand and activate the MR-Glove on the paretic hand [Fig. 2(c)]. Combining with fMRI, we can study the neural mechanism involved when the subject is performing bimanual training based on natural inter-limb synchronization and coordination as well as the reorganization of brain mappings on both the unaffected and affected hemisphere [35]. This control strategy is able to provide insights into the efficacy of bimanual training strategy at the brain level.

A. Actuator Design

A number of research groups have developed soft pneumatic actuators such as PneuNets actuators [36] and fiber-reinforced actuators [37], [38] for the soft robotic glove application. Fiber reinforcement has been proved to be a robust method to constrain the undesired radial expansion, which does not contribute to effective motion during pressurization. However, this method limits the bending capability of the actuators; as a result, higher pressure is needed to achieve desired bending.

In this paper, we developed a new type of soft fabric-regulated pneumatic actuators with a corrugated outer fabric layer which could minimize the excessive budging and provide better bending capability compared to soft actuators used in previous studies [39], [40]. This corrugated fabric layer allows a certain degree of initial radial expansion to initiate bending and then constrains any further radial expansion [Fig. 3(a)]. A two-part 3D-printed mold is required to fabricate the actuators. The lower-part mold (chamber mold) is used to create a pneumatic chamber inside the actuators, which will inflate

upon pressurization, while the upper-part mold (outer layer mold) is used to impose the corrugated outer layer at the top of the actuators. The detailed description of the fabrication process can be found in the Supplementary Information S1.

Upon pressurization, the top surface of the actuators expands due to the inflation of the embedded pneumatic chamber. The strain-limiting fabric restricts the elongation at the bottom surface. This results in the bending of the actuators upon actuation. Combining both stretchable and strain-limiting fabrics at the bottom surface [Fig. 3(b)], the actuators can achieve bending and extending motions [Fig. 3(c)]. The bending motion can support the flexion at the finger joints and the extending motion can offset the increased distance due to skin stretching when the finger is flexing.

B. MR-Glove Prototype Integration

The overall structure of the device is a glove with five actuator-finger pockets attached on the dorsal side (Fig. 1). The glove serves as a compliant interface to the human hand and provides minimal mechanical impedance to the finger motion when being worn. Open palm design is adopted for easy donning and doffing of the glove.

The soft actuators can be easily inserted into the actuator pockets. The actuator pockets are made from stretchable lycra fabrics, which serve as second constraining layers for the actuators. Each actuator is isolated with respect to the others, thus the assistance of each finger can be achieved independently. This allows for execution of different simulated ADL tasks. Silicone connecting tubes of the actuators are connected to an external pneumatic source.

The entire device (the glove with all the actuators and connecting tubes) weighs less than 180 g. Upon air pressurization, the device actuates and assists with hand grasping. Upon depressurization, the actuators act as an elastomeric return spring. The elastic forces of the elastomer serve as a passive return mechanism that brings the fingers to the open hand state [41]. In this paper, we consider only one task-specific exercise during rehabilitation, which is hand grasping. Actuation of the thumb is not considered.

III. Performance of MR-Glove

A. Force Tests of Actuator Outside MR Environment

The total grip force applied by the actuators during pressurization was measured using a universal testing machine (Model 3345, Instron, MA, USA). A cylinder with diameter of 75 mm was positioned at the palmar side of the glove [Fig. 4(a)]. Four actuators were pressurized to 120 kPa to enclose and grasp the cylinder. The glove was anchored to the table and the cylinder was pulled upward by the Instron at a fixed velocity (8 mm/s) until the cylinder was released from the actuators' grasp. The experiment was repeated five times and the results were averaged and shown in Fig. 5(a). The actuators had a total grip (resistive) force of 41.01 ± 2.73N. Considering a friction coefficient of 0.46 [42], the actuators were able to generate a total friction force of 18.88 N to counteract the weight of an object. As the objects of daily

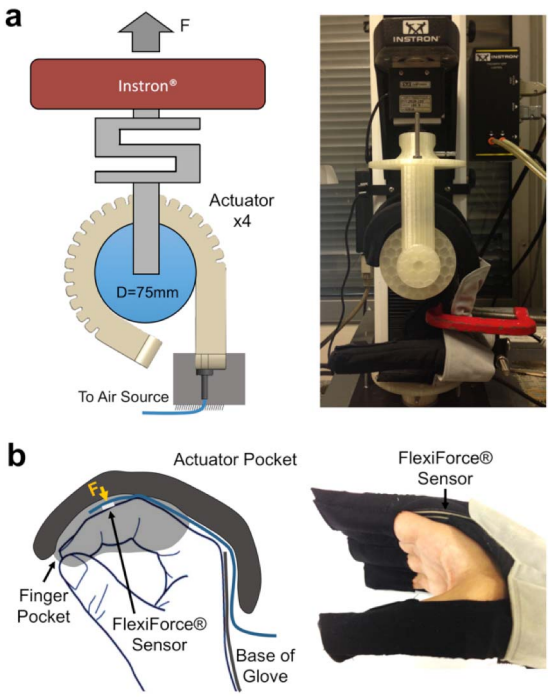

Fig. 4. Force setup to measure (a) total grip force applied by four actuators during pressurization and (b) force exerted by single actuator on the intermediate phalanx of the index finger.

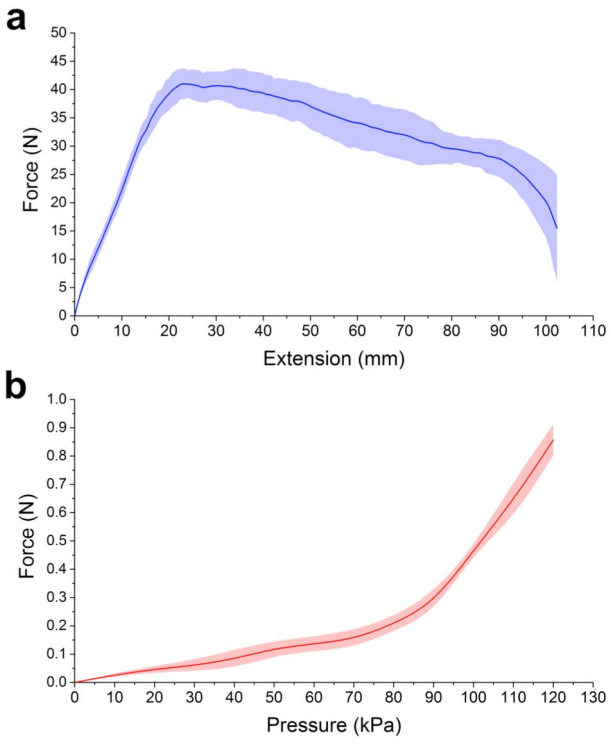

Fig. 5. (a) Load-extension response of four actuators gripping a cylinder with 75 mm diameter. (b) Force-pressure relationship of a single actuator on the intermediate phalanx of the index finger.

living do not weigh more than 1.5 kg [43], the friction force was found to be sufficient to lift most of the objects.

Assuming the total grip force was equally distributed by four actuators, each actuator was able to apply a grip force of 10.25 N during pressurization. According to a previous study,

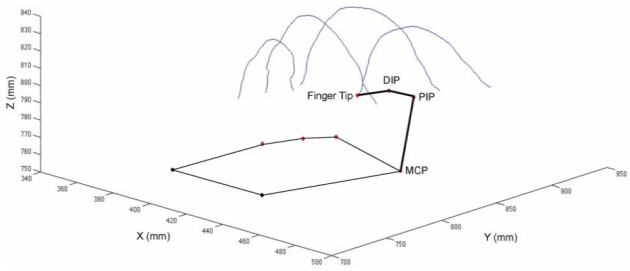

Fig. 6. Measured trajectories for the index, middle, ring, and small fingers during finger flexion.

the estimated minimum force required to achieve a palmar grasp and manipulate most objects of daily living is 8 N [28]. Therefore, the grasping force generated by each actuator was thus considered to be sufficient to actuate the fingers. Compared to the fiber-reinforced actuators which are made from Elastosil M4601 (Shore Hardness 28 A) and operates at the pressure range of 275–375kPa [28], the actuators developed in this study were able to achieve higher force output at lower pressure, with a less stiff material (Shore Hardness 10 A). With this advantage, the selection of the electro-pneumatic components such as pump and valves is less stringent.

In a second experiment, the force exerted by an actuator on the intermediate phalanx of the index finger was measured with a flexible force sensor (FlexiForce A201, Tekscan, MA, USA) [Fig. 4(b)]. The force increased with increasing pressure [Fig. 5(b)]. The maximum force was 0.86 ± 0.06N at 120 kPa.

B. Range of Motion of MR-Glove outside MR Environment

An optical-based motion analysis system with eight cameras (Vicon Motion System Ltd., U.K.) was used to capture the kinematic of the finger of a healthy subject. Twelve reflective markers were attached to the glove according to the VICON Right Hand Model. The motion profile of the index finger was tracked in this case as the index finger provided the best line of sight for the cameras to detect the markers. The markers were attached to the index finger at locations corresponding to the fingertip, distal interphalangeal (DIP), proximal interphalangeal (PIP), and metacarpophalangeal (MCP) joints (Fig. 6). The trajectories of the markers were recorded by the cameras at a sampling rate of 100 Hz.

Three sessions were conducted for the subject. In the first session (Condition 1), the subject was asked to actively flex and extend his fingers with the presence of the glove but without the presence of the actuators. In the second session (Condition 2), the subject was asked to actively flex and extend his fingers with the presence of both the glove and the actuators. In the third session (Condition 3), the subject was instructed to relax his muscles and the finger flexion was assisted by the actuation of the soft actuators at 120 kPa. Five trials were repeated for each session. The kinematics data were averaged across five trials and analyzed using VICON BodyBuilder and VICON BodyLanguage (Vicon Motion System Ltd., U.K.) with customized code to calculate the ROM of each joint. The mean and standard deviation (SD) of the ROM across the five trials were reported in Table I.

TABLE I
PEAK JOINT FLEXION ANGLE

Condition	MCP (°)	PIP (°)	DIP (°)
1: Active (without actuator)	88.9±4.9	94.5±0.8	36.7±0.8
2: Active (with actuators)	86.6±1.3	88.2±1.9	34.6±0.7
3: Passive (assisted by actuators)	79.2±4.1	84.3±6.8	46.4±9.9

The results shown in Table I for conditions 1 and 2 indicate that the presence of the actuators did not affect the ROM of each joint significantly. In the case of condition 3, our results indicate that the MR-Glove could achieve at least 95.4% of the active ROM for each joint. The peak flexion angles of DIP in both Condition 1 and 2 were smaller than that in Condition 3 because the subject did not intentionally flex his DIP joint to its maximum active ROM, which is $84.0 \pm 8.5°$ reported in the literature [44]. The achievable ROM in Condition 3 was found to be within the functional ROM of joints reported in the literature [44]. These results demonstrate that the MR-Glove is able to support the ROM of a human hand.

C. Controller Design and Mechanical Implementation

An electro-pneumatic actuation system was utilized in order to allow for actuation of the MR-Glove. The control system that controls the individual digital actuations of the MR-Glove system is based on an Arduino Mega micro-controller. The microcontroller is connected to a series of current drivers. The closed loop pneumatic actuation and sensing system consists of air pressure sensors (MPX5500DP, Freescale, TX, USA) for air pressure regulation within each actuator, miniature solenoid valves (X-Valve, Parker Hannifin Corp., OH, USA), and a miniature air compressor (AF186, Airbrush, SG).

An industry-standard Proportional Integral Derivative (PID) control algorithm is used ensure that the measured air pressure (P) of the actuators are close to desired air pressure (P_{ref}). This algorithm is used on 97% of all control loops used in process control in refining, chemical and pulp and paper industries [45] where physical models can be difficult or laborious to obtain. This is especially so in our case where flexure is non-trivial to model. Hence, the control scheme has to be able to accommodate a black-box model. In addition, control loop tuning is simple as the changes in transient performance correlate easily with changes in control gains. For these reasons, the PID algorithm was selected for this work. A diagram showing the control loop and the mechanical connections is shown in Fig. 7.

The coupled current driver utilizes a Pulse Width Modulation (PWM) voltage scheme to indirectly control the valve current. The PID control scheme was implemented on the microcontroller with a sampling frequency of 100 Hz. A miniature solenoid valve with a nominal response time of 20 ms and PWM frequency of 50 Hz was used for each

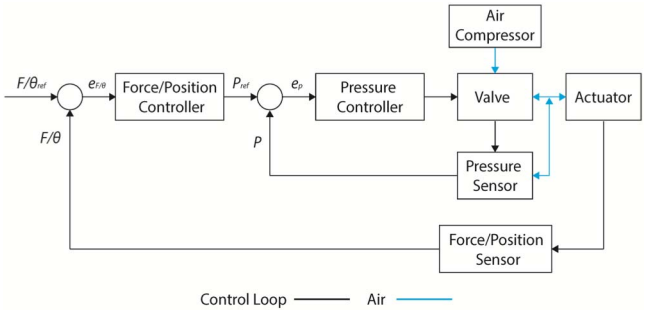

Fig. 7. Control implementation for each individual soft actuator.

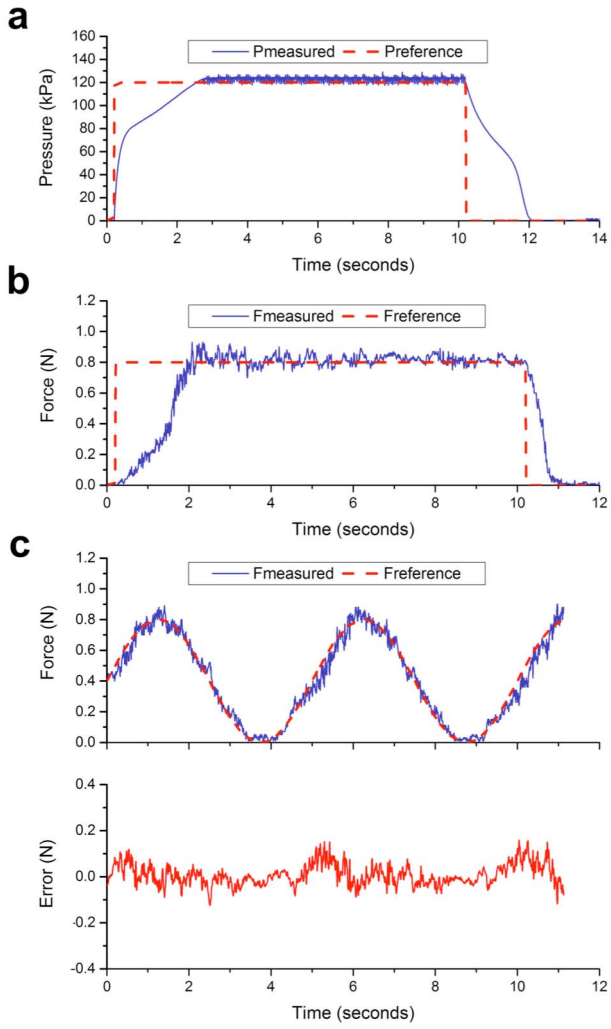

Fig. 8. (a) Pressure and (b) force step response of the controller implemented on the MR-Glove. (c) Sinusoidal tracking performance with a force reference signal of 0.2 Hz.

actuator. The valve was connected to the actuator where the inlet was in line with the pressure sensor and the outlet with air exhaust.

In a step pressure tracking experiment, the desired pressure P_{ref} was set at 120 kPa, which was the pressure that corresponded to full finger flexion based on the results from ROM test. The actuator for the index finger of the MR-Glove was pressurized from 0 kPa to 120 kPa. The control loop was tested in a step response experiment [Fig. 8(a)]. The control

Fig. 9. (a) FBG sensors integrated with MR-Glove. (b) Complete MR-Glove system with electro-pneumatic control system, FBG sensor array, and FBG Interrogator (FBG-Scan 804D).

parameters are selected as $K_{\text{p}} = 20$, $K_{\text{i}} = 0.7$, and $K_{\text{d}} = 0.1$. When excited by a step input with $P_{\text{ref}} = 120$kPa, the closed loop system had a rise time of 1.79 s and a settling time (5%) of 2.08 s, with a steady state error of 3.21 kPa (2.68%).

Additionally, step and sinusoidal force tracking experiments were conducted to evaluate the force control of the system with the setup described in Section III-A. The control parameters are selected as $K_p = 20$, $K_i = 25$ and $K_d = 0.1$. When excited by a step input of 0.8 N, the closed loop system had a rise time of 1.20 s, a settling time (5%) of 1.68 s, with a steady state error of 0.03 N [Fig. 8(b)]. The closed loop system bandwidth was found to be 0.29 Hz. In the sinusoidal experiment [Fig 8(c)], the system was able to track a force reference signal of 0.2 Hz with root-mean-square error of 0.05N (6.25%).

D. Tracking of Hand Kinematics

To enable tracking of hand kinematics during MR experiments, optical fiber Bragg gratings (FBG) sensors (DTG-A3A4-E00, FBGs, Geel, Belgium) were integrated in the MR-Glove (Fig. 9). FBG sensors are optical fiber sensors sensitive to strain. Therefore, they can be used as a strain gauge sensor that applied to each phalanx joint in order to measure the skin stretch during hand closing and opening and translate the strain to joint angle. In this work, four fibers were used. Three FBG sensors, which corresponded to MCP, PIP, and DIP joints, were placed in each fiber and occupied a small bandwidth. The detailed description of the specification and integration of FBG sensors can be found in the Supplementary Information S2 and S3.

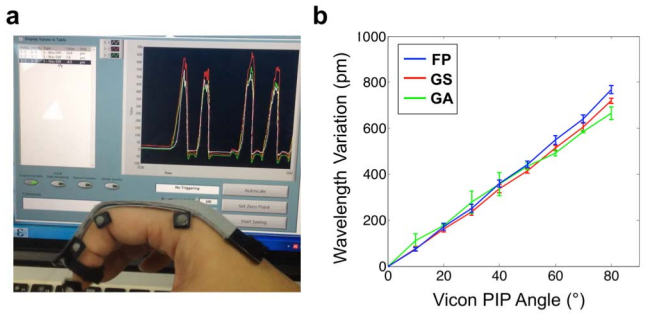

Fig. 10. (a) Example of the experiment setup to determine (b) the relationship between the wavelength variation and the reference PIP joint angle under three conditions (FP: voluntary movements with sensors alone; GS: voluntary movements with sensors integrated with the glove and the glove was silent; GA: glove-assisted movements).

The reflected Bragg signal of a FBG sensor changes its spectral component as a function of the strain. The Bragg signal wavelength equation is expressed as

$$\lambda_B = 2 \cdot n_{eff} \cdot \Lambda_B \tag{1}$$

where n_{eff} is the effective refraction index of the fiber core and Λ_B is the grating pitch. When a spectrally broadband source (interrogator) injects light into the fiber, a narrow spectral component is reflected back by the grating. The strain response results from the physical elongation of the sensor will induce the changes in both refraction index and grating pitch. Thus the Bragg wavelength λ_B changes accordingly. For a more detailed working principle of FBG sensors, the authors refer to the work done by da Silva *et. al* [46].

To validate the accuracy of kinematics measurement of the FBG sensors, the relationship between the wavelength variation and the reference joint angles was determined under three conditions (FP: voluntary movements with sensors alone; GS: voluntary movements with sensors integrated with the glove and the glove was silent; GA: glove-assisted movements) using the motion analysis system (Vicon Motion System Ltd., U.K.) described in Section III-B (Fig. 10). As the subject flexed the fingers, a positive wavelength deviation was observed, and vice versa. The capability of tracking hand kinematics during MR-experiments was demonstrated in Fig. 11(c) and (d).

The small difference between the calibration curves might be due to a transverse and uniform distributed forces applied on the sensors when the sensors were integrated with the glove and the glove was activated, which induced refractive index changes and by consequence a birefringence [47]. If the sensors were integrated directly into the actuators, the force–related deformations in the pneumatic chamber will aggravate the birefringence effects. To mitigate this phenomenon, instead of integrating the sensors directly into the actuators, they were embedded into a finger patch, which was placed in between the fingers and the actuators (Supplementary Information S3). With this configuration, pressurization of the pneumatic chamber will not apply transverse forces directly to the sensors, but instead, apply the forces directly to the fingers and flex the finger joints. The longitudinal strain resulted from finger bending will be captured by the sensors. Prior to the fMRI experiments, initial calibration under three conditions (i.e. FP, GS, and GA) is also required in order to capture the finger kinematics properly.

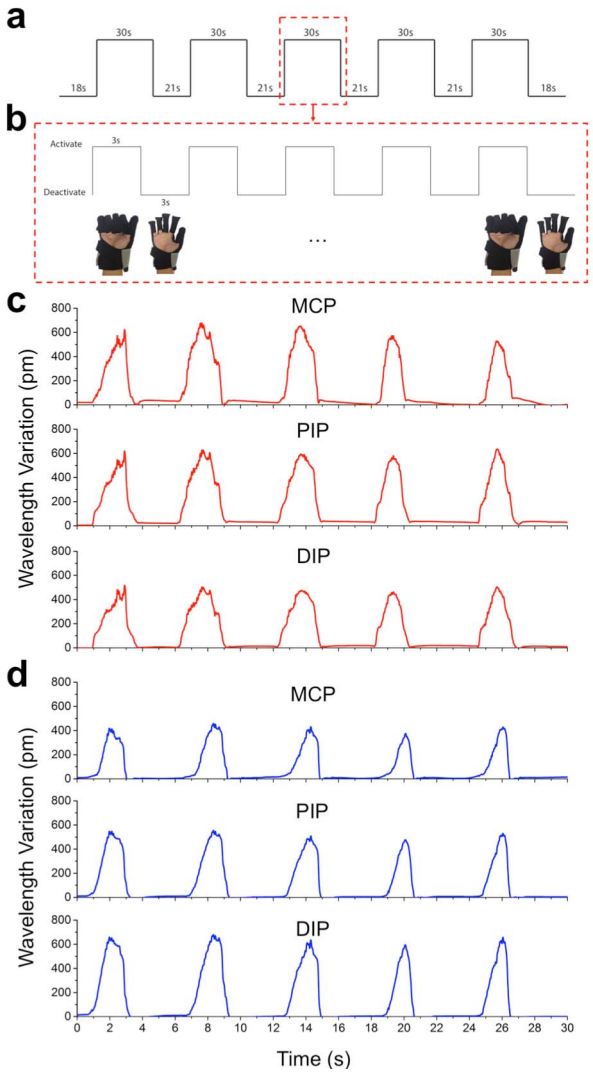

Fig. 11. (a) Experimental paradigm. MRC-Glove was activated during the five 30 s-blocks. (b) In each 30 s-block, the actuators were activated and deactivated for five times. Both the activation and deactivation time were 3 s. The P_{ref} was set at 120 kPa, which was the pressure that corresponded to full finger flexion based on the results from ROM test outside the MR environment. The wavelength variation of the FBG sensors on MCP, PIP, DIP joints when (c) the subject flexed his fingers voluntarily (Condition GS) and (d) the subject was instructed to relax his muscles and the finger flexion was assisted by the actuation of the soft actuators at 120 kPa (Condition GA).

IV. MR Compatibility Tests of MR-Glove

To investigate the MR compatibility and the possibility of MR-Glove causing artifacts and degradation to the MR images in the MR environment, a series of phantom and human tests were conducted.

A. Experimental Setup

The experiments were performed on a Siemens MAGNETOM Tim Trio 3T MRI system. Structural MR images were acquired using magnetization-prepared rapid

gradient-echo (MPRAGE). The acquisition parameters were: FOV 256×256 mm^2, matrix 256×256, slice thickness 1 mm, slice number per slab 176, TR/TE = 1900/2.52 ms, echo spacing time 7.5 ms, bandwidth 170 Hz/pixel. Parallel acquisition was conducted in the GRAPPA mode, with reference line phase encoding (PE) = 24, and an acceleration factor of 1. TI_{EFF} of the MP-RAGE sequence, which defined as the time between the inversion recovery pulse and k-space center acquisition, was set at 900 ms with a flip angle of 9°. The total acquisition time for each test was 4 min 26 s.

Functional MR images were acquired using a gradient echo-planar (GE-EPI) sequence. The GE-EPI was acquired with the following parameters: FOV 220×220 mm^2, matrix 64x64, slice thickness 3.4 mm, number of slices= 42 acquired in an interleaved fashion, TR/TE = 3000/30 ms, echo spacing time 0.73 ms, EPI factor = 64, bandwidth 1502 Hz/pixel, and number of measurements= 89.

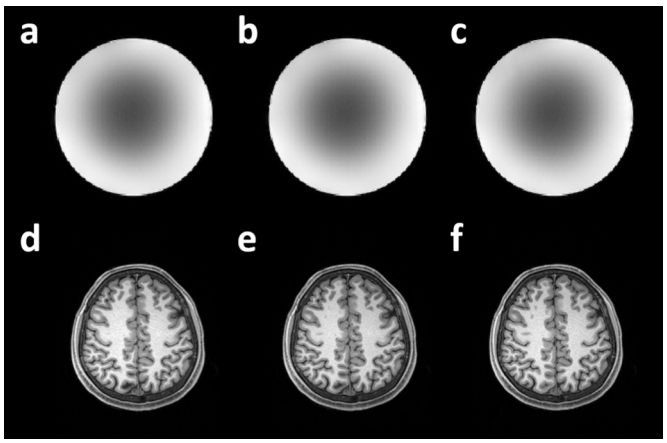

Fig. 12. Effect of MR-Glove on MPRAGE phantom and brain images: (a, d) Control (NG). (b, e) Presence of MR-Glove, not operating (GS). (c, f) Presence of MR-Glove, operating (GA).

TABLE II
SNR FOR MPRAGE PHANTOM IMAGES

Condition	Signal (a.u.[a].)	SNR	P-Value
NG: Control	1522.0±45.1	257.7±18.6	
GS: Presence of MR-Glove (Not Operating)	1522.7±45.5	256.5±13.1	0.94
GA: Presence of MR-Glove (Operating)	1521.6±46.0	256.3±8.2	0.91

[a]a.u.=arbitrary unit

Signal and SNR data were measured and averaged across 11 slices in transverse section. Each slide consisted of 24496 voxels.

B. Phantom Test

To test the compatibility of MR-Glove under MR environment, phantom tests were conducted. The variations of signal to noise ratio (SNR) of the MPRAGE structural images and temporal signal to noise ratio (tSNR) of the EPI functional images were computed. A Siemens standard spherical phantom composed of NiSO4x6H2O was used as a phantom. Phantom control images (NG: No Glove) were first acquired without the presence of MR-Glove. In the second trial (GS: Glove Silent), MR-Glove was placed on the scanner table, 25 cm in front of the cylindrical phantom. Silicon pneumatic tubes (Length: 4 m) were connected to the actuators and the distal ends of the tubes were connected to the electro-pneumatic actuation system located outside the MR room. The phantom images were then acquired with the presence of the MR-Glove. The phantom remained stationary throughout the entire tests. In the third trial (GA: Glove Active), the phantom images were obtained in the presence of MR-Glove, with actuators activated according to the preset experimental paradigm outlined in Fig. 11(a) and (b).

1) MPRAGE Structural Phantom Images:: SNR of the phantom images under three conditions (Condition 1: Control, Condition 2: Presence of MR-Glove, and Condition 3: Presence of activated MR-Glove) were computed in the image domain. The SNR was computed according to NEMA method 1 (N1) [48].

In the N1 method, two phantom images were acquired with the same imaging parameters within 5 min of each other. The signal was defined as the average pixel value of a region of interest (ROI) encompassing 75% of the signal-producing region of the average image of two images. To obtain the noise, the two images were subtracted to produce a third image. A ROI, which was used in the above signal calculation, was drawn in the third image. The standard deviation (SD) from this ROI was taken as the image noise

$$SD = \left[\frac{\sum_{i=1}^{n} \sum_{j=1}^{m_i} \left(R\left(i, j\right) - \bar{R} \right)^2}{\sum_{i=1}^{n} \left(m_i \right) - 1} \right]^{\frac{1}{2}} \tag{2}$$

where $R(i, j)$ is the individual pixel value within the ROI, $\bar{R}$ is the average pixel value of the ROI, and i and j are pixel numbers in the row and column direction.

The SD was then divided by $\sqrt{2} = 1.41$ Gaussian distribution correction factor [49].

The MPRAGE phantom images under the three conditions are presented in Fig. 12(a)–(c). The phantom signal remained stable despite the introduction and operation of the MR-Glove (Table II). The mean signal intensity deviated less than 0.05% from the control condition. Two-tailed Student's t tests (P = 0.05) were conducted to compare the values of mean SNR under condition GS and GA to control condition NG. Results showed that there was no statistically significant difference between the control condition NG and condition GS, as well as between the control condition NG and condition GA.

2) EPI Functional Phantom Images:: tSNR was used to access the introduction of temporal fluctuations in the fMRI signal due to a particular experimental condition. This measure, which was proposed in [50], [51] and conventionally used in MR-compatible robotics literature [52]–[54], was defined on a voxel-wise basis as the mean signal intensity divided by the temporal standard deviation (fluctuation noise).

A ROI was defined as a rectangular set of $16 \times 16 \times 16$ adjacent voxels in the center of the phantom, resulting in a total of 4096 voxels. For each individual voxel i, the signal intensity was averaged across the time series, with mean $\bar{S}_i$. To calculate

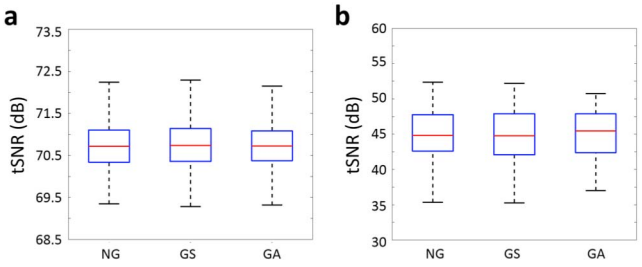

Fig. 13. Box plot describing the distribution of tSNR in different experimental conditions during (a) phantom and (b) human tests. (Red line: the median, box edges: the $25^{th}(q_1)$ and 75^{th} (q_3) percentiles. Whiskers extend to q_3 +1.5(q_3–q_1) and q_1-1.5(q_3-q_1).

the fluctuation noise, the time series for each voxel i was detrended using a linear regression. The fluctuation noise for each voxel i is the SD of the residuals after detrending.

tSNR (expressed in dB) for each voxel i was calculated as

$$tSNR_i = 20\log_{10}\frac{\bar{S}_i}{SD_i} \tag{3}$$

The measured distributions of tSNR from all 4096 voxels were subject to non-parametric Kruskal-Wallis test to evaluate the significance of the effect of a particular experimental condition on tSNR. This statistical analysis was used to test the null hypothesis stating that the mean rank of samples (voxels) for the given measure of interest (tSNR), in each experimental condition (NG, GS, GA), is the same [53].

The results showed that the effect of the experimental condition on tSNR was not significant at the $p < 0.05$ significance level ($p = 0.18$) [Fig. 13(a)]

C. Human Test

Human tests were conducted with a healthy human subject who underwent hand-grasping exercise assisted by MR-Glove. MR-Glove was activated according to the preset experimental paradigm [Fig. 11(a) and (b)]. Both the MPRAGE structural images and the EPI functional images were acquired with the subject lying in the normal supine position in the MR scanner. The images were acquired under three conditions, NG: Control (No MR-Glove in the scanner), GS: Presence of MR-Glove in the scanner and the subject was wearing the glove, and GA: Presence of MR-Glove in the scanner. The actuators were activated and the finger joints of the subject were actuated.

1) MPRAGE Structural Brain Images:: SNR of the MRRAGE brain images were calculated according to the N1 method. ROIs were drawn on each image slide over the largest region of white matter in the central area of the brain axially on both the left and right sides [49]. The MPRAGE structural brain images under the three conditions are presented in Fig. 12(d)–(f). The brain signal remained stable despite the introduction and operation of the MR-Glove. The mean signal intensity deviated less than 0.77% from the control condition NG. The values of mean SNR and its SD were computed and reported in Table III. Simple two-tailed paired t-tests ($p = 0.05$) comparing condition GS and condition GA to control condition NG did not reach statistical significance.

TABLE III
SNR FOR MPRAGE STRUCTURAL BRAIN IMAGES

Condition	Signal (a.u.[a].)	SNR	P-Value
NG: Control	325.7±16.5	38.6±2.6	
GS: Presence of MR-Glove (Not Operating)	325.5±16.1	38.3±4.6	0.86
GA: Presence of MR-Glove (Operating)	328.2±15.8	37.9±2.9	0.55

[a]a.u.=arbitrary unit

Signal and SNR data were measured and averaged across 11 slices in transverse section.

2) EPI Functional Brain Images:: tSNR was calculated using the method described in the phantom test. Similarly, the measured distributions of tSNR were subject to non-parametric Kruskal-Wallis test. The results showed that the effect of the experimental condition on tSNR was not significant at the $p < 0.05$ significance level ($p = 0.86$) [Fig. 13(b)].

V. DISCUSSION AND CONCLUSION

A MR-compatible soft robotic glove using soft pneumatic actuators was proposed for hand rehabilitation, particularly task-specific exercises. Force tests with the actuators showed that they were able to provide a total grip force of 41.01 N and actuate the finger joints with at least 95.4% of active ROM. The ROM experiment demonstrated that the MR-Glove was able to support the ROM of a human hand. MR-compatible FBG sensors were integrated with the MR-Glove in order to serve as real-time hand kinematic tracking elements that are able to quantify the movement of the finger joints in the MR environment. Phantom and human tests were conducted with a MRI system in order to evaluate the MR-compatibility of the MR-Glove. Our results from the phantom and human tests demonstrated that there was no significant degradation effect and artifacts in the MR images with the introduction and operation of the MR-Glove.

The closed-loop pressure and force control presented in this work has been successfully implemented in line with previous works, which demonstrated the ease of actuator controllability [24], [28]. To be specific, closed-loop performance of the MR-Glove has comparable system bandwidth and step response characteristics to that presented in [28]. The actuation frequency of the MR-Glove (0.2–0.3 Hz) is also comparable to the full range of motion frequency of typical rehabilitation exercises for the finger (<0.5 Hz) [28], [55].

As the glove is pneumatically actuated, it suffers from long delay and limited bandwidth [16]. As a result, it might not suitable for fMRI studies of applications involving fine motor control and highly dynamic interactions with the hand and fingers [56]. Therefore, we foresee that the MR-Glove will be suitable for applications with simple tasks and control schemes, such as performing simple simulated ADL tasks (hand pinching, grasping and opening) using time-triggered and bimanual control strategies. On a positive note, as most of manual interventions during physiotherapy sessions are carried out meticulously to avoid incidental damage secondary to sudden or brisk movement on stiffened joints or paralyzed

muscles, by maintaining the lead time between sensing and actuation, the patient can expect the next move and prepare to respond comfortably. The system bandwidth is limited by compressibility of the air, the response time (20 ms) and the flow rate (<4 slpm) of current valves. To increase bandwidth and reduce delay, compressed air supplies with faster flow rate as well as valves with faster flow rate and response time will be selected in the future. The design of the actuators will be further optimized in order to reduce their operating pressure and increase their actuation speed.

The limitation of the current work is that the MR-Glove applies forces to flex the finger and assists passive finger extension with the elastic properties of the actuators and the elastic textile materials of the actuator pockets. For patients with increased flexor tone and spasticity (Modified Ashworth Scale $> 1+$), this passive extension mechanism might not have enough force to unclench their hand or extend their fingers. In the future, soft elastomeric actuators that are able to achieve bi-directional actuation will be explored in order to develop a bi-directional soft robotic glove that is capable to provide active flexion and active extension in order to cater for a larger patient population with various hand mobility issues.

The control and sensing has its limitations. It would be ideal to be able to conduct closed-loop position or force (impedance) control. For the force (impedance) control, the challenge is in sensing as force sensors and their associated cabling are ferrous. This hinders their use in a MR environment. For the position control, further work is planned to use the FBG sensors presented in this work as the position feedback in the control loop. Going further, both force and position control strategies will be studied in greater detail. In addition, through offline characterization, sensor fusion can be implemented to infer the actuation force with pressure and position measurements. This is to improve rehabilitation outcomes and to ensure patient safety. Regarding the issue of birefringence due to the gentle forces applied transversely on the sensors when the glove was activated, a proper FBG integration method (such as helically-wrapped FBG sensors around a flexible substrate so that they are flexible in bending and stiff to axial compression [57]) will be required. Additionally, developing a force-strain model that is able to isolate force measurements from the FBG readings will also be considered to mitigate this issue. Nevertheless, we believe that through proper initial calibration, the FBG sensors integrated MR-Glove presented in this study is able to track the finger kinematics sufficiently, as we are looking into fMRI studies that involve simple tasks and control schemes.

To our best knowledge, this is the first study that evaluated the MR-compatibility of a soft robotic device proposed for hand assistive, rehabilitation and task-specific training applications. Based on soft robotics technology, this work offers a new design paradigm for MR-compatible devices that predominantly utilize rigid components such as ultrasonic motors and piezoelectric actuators. The MR-Glove has the potential to increase the benefits of robot-assisted hand therapy by providing portability, lower weight, and safer human-robot interactions. Apart from being able to serve as an assistive device and conduct task specific exercises that simulate ADL, we envision that the MR-Glove can also serve as a useful tool in fMRI motor studies in order to understand the motor performances of the brain and to unravel the effect of robot-assisted therapy during hand rehabilitation.

ACKNOWLEDGEMENT

The authors would like to thank S. Ng, Y. Low, C. Wong, F.-Z. Low, and B. Ang, for their assistance in the MR experiment. H. K. Yap would like to thank NUS Graduate School for Integrative Sciences and Engineering for providing scholarship support.

REFERENCES

[1] S. M. Michaelsen, R. Dannenbaum, and M. F. Levin, "Task-specific training with trunk restraint on arm recovery in stroke: Randomized control trial," *Stroke*, vol. 37, no. 1, pp. 186–192, Jan. 2006.

[2] P. Maciejasz, J. Eschweiler, K. Gerlach-Hahn, A. Jansen-Troy, and S. Leonhardt, "A survey on robotic devices for upper limb rehabilitation," *J. NeuroEng. Rehabil.*, vol. 11, p. 3, Jan. 2014.

[3] P. Heo, G. M. Gu, S.-J. Lee, K. Rhee, and J. Kim, "Current hand exoskeleton technologies for rehabilitation and assistive engineering," *Int. J. Precis. Eng. Manuf.*, vol. 13, no. 5, pp. 807–824, May 2012.

[4] G. Kwakkel, B. J. Kollen, and H. I. Krebs, "Effects of robot-assisted therapy on upper limb recovery after stroke: A systematic review," *Neurorehabil. Neural Repair*, vol. 22, no. 2, pp. 111–121, Sep. 2007.

[5] A. Timmermans, H. A. Seelen, R. D. Willmann, and H. Kingma, "Technology-assisted training of arm-hand skills in stroke: Concepts on reacquisition of motor control and therapist guidelines for rehabilitation technology design," *J. NeuroEng. Rehabil.*, vol. 6, no. 1, p. 1, Jan. 2009.

[6] G. Kwakkel, B. J. Kollen, and H. I. Krebs, "Effects of robot-assisted therapy on upper limb recovery after stroke: A systematic review," *Neurorehabil. Neural Repair*, vol. 22, pp. 21–111, Mar./Apr. 2008.

[7] N. Takeuchi and S.-I. Izumi, "Rehabilitation with poststroke motor recovery: A review with a focus on neural plasticity," *Stroke Res. Treat.*, vol. 2013, p. 13, Apr. 2013.

[8] O. Monchi, H. Benali, J. Doyon, and A. P. Strafella, "Recent advances in neuroimaging methods," *Int. J. Biomed. Imag.*, vol. 2008, p. 218582, May 2008.

[9] H. Chen, J. Epstein, and E. Stern, "Neural plasticity after acquired brain injury: Evidence from functional neuroimaging," *PM&R*, vol. 2, no. 12, pp. S306–S312, Dec. 2010.

[10] N. S. Ward, M. M. Brown, A. J. Thompson, and R. S. J. Frackowiak, "Neural correlates of motor recovery after stroke: A longitudinal fMRI study," *Brain*, vol. 126, no. 11, pp. 2476–2496, Aug. 2003.

[11] A. Wege and G. Hommel, "Development and control of a hand exoskeleton for rehabilitation of hand injuries," in *Proc. IEEE/RSJ Int. Conf. Intell. Robots Syst. (IROS)*, Aug. 2005, pp. 3046–3051.

[12] T. T. Worsnopp, M. A. Peshkin, J. E. Colgate, and D. G. Kamper, "An actuated finger exoskeleton for hand rehabilitation following stroke," in *Proc. IEEE 10th Int. Conf. Rehabil. Robot. (ICORR)*, Jun. 2007, pp. 896–901.

[13] A. Khanicheh *et al.*, "fMRI-compatible rehabilitation hand device," *J. Neuroeng. Rehabil.*, vol. 3, p. 24, Oct. 2006.

[14] J. L. Wilson, M. Jenkinson, I. de Araujo, M. L. Kringelbach, E. T. Rolls, and P. Jezzard, "Fast, fully automated global and local magnetic field optimization for fMRI of the human brain," *Neuroimage*, vol. 17, no. 2, pp. 967–976, Oct. 2002.

[15] T. Fisher *et al.*, "Intraoperative magnetic resonance imaging-conditional robotic devices for therapy and diagnosis," *Proc. Inst. Mech. Eng. H*, vol. 228, no. 3, pp. 303–18, Mar. 2014.

[16] R. Gassert, A. Yamamoto, D. Chapuis, L. Dovat, H. Bleuler, and E. Burdet, "Actuation methods for applications in MR environments," *Concepts Magn. Reson. B, Magn. Reson. Eng.*, vol. 29B, no. 4, pp. 191–209, Oct. 2006.

[17] R. Riener, T. Villgrattner, R. Kleiser, T. Nef, and S. Kollias, "fMRI-Compatible electromagnetic haptic interface," *Proc. IEEE Eng. Med. Biol. Soc.*, Jan. 2006, pp. 7024–7027.

[18] J. Z. Liu, T. H. Dai, T. H. Elster, V. Sahgal, R. W. Brown, and G. H. Yue, "Simultaneous measurement of human joint force, surface electromyograms, and functional MRI-measured brain activation," *J. Neurosci. Methods*, vol. 101, no. 1, pp. 49–57, Aug. 2000.

[19] M. Flueckiger, M. Bullo, D. Chapuis, R. Gassert, and Y. Perriard, "fMRI compatible haptic interface actuated with traveling wave ultrasonic motor," in Proc. *Ind. Appl. Conf. 40th IAS Annu. Meet. Conf. Rec.*, Oct. 2005, pp. 2075–2082.
[20] J. Hidler, T. Hodics, B. Xu, B. Dobkin, and L. G. Cohen, "MR compatible force sensing system for real-time monitoring of wrist moments during fMRI testing," *J. Neuroscience Methods*, vol. 155, no. 5, pp. 300–307, Sep. 2006.
[21] A. Khanicheh, D. Mintzopoulos, B. Weinberg, A. A. Tzika, and C. Mavroidis, "MR_CHIROD v.2: Magnetic resonance compatible smart hand rehabilitation device for brain imaging," *IEEE Trans. Neural Syst. Rehabil. Eng.*, vol. 16, no. 1, pp. 91–98, Mar. 2008.
[22] D. Rus and M. T. Tolley, "Design, fabrication and control of soft robots," *Nature*, vol. 521, pp. 467–475, May 2015, doi: 10.1038/nature14543.
[23] H. In, B. B. Kang, M. Sin, and K. J. Cho, "Exo-glove: A wearable robot for the hand with a soft tendon routing system," *IEEE Robot. Autom. Mag.*, vol. 22, no. 1, pp. 97–105, Mar. 2015.
[24] K. Tadano, M. Akai, K. Kadota, and K. Kawashima, "Development of grip amplified glove using bi-articular mechanism with pneumatic artificial rubber muscle," in *Proc. IEEE Int. Conf. Robot. Autom. (ICRA)*, May 2010, pp. 2363–2368.
[25] D. Sasaki, T. Noritsugu, M. Takaiwa, and H. Yamamoto, "Wearable power assist device for hand grasping using pneumatic artificial rubber muscle," in *Proc. IEEE Int. Workshop Robot Human Interact. Commun.*, Sep. 2004, pp. 655–660.
[26] L. Connelly, Y. Jia, M. L. Toro, M. E. Stoykov, R. V. Kenyon, and D. G. Kamper, "A pneumatic glove and immersive virtual reality environment for hand rehabilitative training after stroke," *IEEE Trans. Neural Syst. Rehabil. Eng.*, vol. 18. Oct. 2010, pp. 551–559.
[27] Y. Kadowaki, T. Noritsugu, M. Takaiwa, D. Sasaki, and M. Kato, "Development of soft power-assist glove and control based on human intent," *J. Robot. Mechatron.*, vol. 23, no. 2, pp. 281–291, Feb. 2011.
[28] P. Polygerinos, Z. Wang, K. C. Galloway, R. J. Wood, and C. J. Walsh, "Soft robotic glove for combined assistance and at-home rehabilitation," *Robot. Auto. Syst.*, vol. 73, pp. 135–143, Nov. 2015.
[29] H. K. Yap, J. H. Lim, F. Nasrallah, J. C. H. Goh, and R. C. H. Yeow, "A soft exoskeleton for hand assistive and rehabilitation application using pneumatic actuators with variable stiffness," in *IEEE Int. Conf. Robot. Autom. (ICRA)*, May 2015, pp. 4967–4972.
[30] P. Maeder-York *et al.*, "Biologically inspired soft robot for thumb rehabilitation," *J. Med. Devices*, vol. 8, no. 2, p. 020933, Jun. 2014.
[31] P. Polygerinos, K. C. Galloway, E. Savage, M. Herman, K. O. Donnell, and C. J. Walsh, "Soft robotic glove for hand rehabilitation and task specific training," in *Proc. IEEE Int. Conf. Robot. Autom. (ICRA)*, May 2015, pp. 2913–2919.
[32] J. Sulzer *et al.*, "Delineating the whole brain bold response to passive movement kinematics," in *Proc. IEEE Int. Conf. Rehabil. Robot.*, Jun. 2013, pp. 1–5.
[33] L. Marchal-Crespo and D. J. Reinkensmeyer, "Review of control strategies for robotic movement training after neurologic injury," *J. Neuroeng. Rehabil.*, vol. 6, p. 20, Jun. 2009.
[34] C. D. Takahashi, L. Der-Yeghiaian, V. Le, R. R. Motiwala, and S. C. Cramer, "Robot-based hand motor therapy after stroke," *Brain*, vol. 131, pp. 425–437, Dec. 2008.
[35] A. R. Luft *et al.*, "Repetitive bilateral arm training and motor cortex activation in chronic stroke: A randomized controlled trial," *JAMA*, vol. 292, no. 15, pp. 1853–1861, Oct. 2004.
[36] B. Mosadegh *et al.*, "Pneumatic networks for soft robotics that actuate rapidly," *Adv. Funct. Mater.*, vol. 24, no. 15, pp. 2163–2170, Apr. 2014.
[37] K. C. Galloway, P. Polygerinos, C. J. Walsh, and R. J. Wood, "Mechanically programmable bend radius for fiber-reinforced soft actuators," in *Proc. 16th Int. Conf. Adv. Robot. (ICAR)*, Nov. 2013, pp. 1–6.
[38] P. Polygerinos *et al.*, "Modeling of soft fiber-reinforced bending actuators," *IEEE Trans. Robot.*, vol. 31, no. 3, pp. 778–789, May 2015.
[39] Y. Elsayed *et al.*, "Finite element analysis and design optimization of a pneumatically actuating silicone module for robotic surgery applications," *Soft Robot.*, vol. 1, no. 4, pp. 255–262, Dec. 2014.
[40] H. K. Yap, J. H. Lim, F. Nasrallah, J. C. H. Goh, and C.-H. Yeow, "Characterisation and evaluation of soft elastomeric actuators for hand assistive and rehabilitation applications," *J. Med. Eng. Technol.*, vol. 40,no. 4 pp.199–209, May 2016.
[41] L. T. Philip and T. Jason, "Entropic forces-making the connection between mechanics and thermodynamics in an exactly soluble model," *Eur. J. Phys.*, vol. 34, no. 3, p. 729, Apr. 2013.
[42] M. Zhang and A. F. T. Mak, "In vivo friction properties of human skin," *Prosthet. Orthot. Int.*, vol. 23 no. 2, pp. 135–141, Jan. 1999.
[43] K. Matheus and A. M. Dollar, "Benchmarking grasping and manipulation: Properties of the objects of daily living," in *Proc. IEEE/RSJ Int. Conf. Intell. Robots Syst. (IROS)*, Oct. 2010, pp. 5020–5027.
[44] G. I. Bain, N. Polites, B. G. Higgs, R. J. Heptinstall, and A. M. McGrath, "The functional range of motion of the finger joints," *J. Hand Surg. Eur.*, vol. 40, no. 4, pp. 11–406, May 2015.
[45] L. Desborough and R. Miller, "Increasing customer value of industrial control performance monitoring-Honeywell's experience," in *Proc. AIChE Symp.*, Jan. 2002, pp. 169–189.
[46] A. F. D. Silva, A. F. Goncalves, P. M. Mendes, and J. H. Correia, "FBG Sensing glove for monitoring hand posture," *IEEE Sensors J.*, vol. 11, no. 10, pp. 2442–2448, Apr. 2011.
[47] J. Zhao, X. zhang, Y. Huang, and X. Ren, "Experimental analysis of birefringence effects on fiber Bragg gratings induced by lateral compression," *Opt. Commun.*, vol. 229, nos, 1–6, pp. 203–207, Jan. 2004.
[48] National Electrical Manufacturers Association, "Determination of signal-to-noise ratio (SNR) in diagnostic magnetic resonance imaging," NEMA Standards Publication MS1-2008, 2008.
[49] F. L. Goerner and G. D. Clarke, "Measuring signal-to-noise ratio in partially parallel imaging MRI," *Med. Phys.*, vol. 38, no. 9, pp. 5049–5057, Sep. 2011.
[50] L. Friedman and G. H. Glover, "Report on a multicenter fMRI quality assurance protocol," *J. Magn. Reson. Imag.*, vol. 23, no. 6, pp. 827–839, Jun. 2006.
[51] L. Friedman and G. H. Glover, "Reducing interscanner variability of activation in a multicenter fMRI study: Controlling for signal-to-fluctuation-noise-ratio (SFNR) differences," *Neuroimage*, vol. 33, no. 2, pp. 471–481, Nov. 2006.
[52] N. Yu, N. Estévez, M. C. Hepp-Reymond, S. S. Kollias, and R. Riener, "fMRI assessment of upper extremity related brain activation with an MRI-compatible manipulandum," *Int. J. Comput. Assist. Radiol. Surg*, vol. 6, no. 3, pp. 447–455, May 2011.
[53] F. Sergi, A. C. Erwin, and M. K. O'Malley, "Interaction Control Capabilities of an MR-Compatible Compliant Actuator for Wrist Sensorimotor Protocols During fMRI," *IEEE/ASME Trans. Mechatron.*, vol. 20, no. 6, pp. 2678–2690, Dec. 2015.
[54] A. Erwin, M. K. O. Malley, D. Ress, and F. Sergi, "Development, control, and MRI-compatibility of the MR-softwrist," in *Proc. IEEE Int. Conf. Rehabil. Robot. (ICORR)*, Aug. 2015, pp. 187–192.
[55] P. Agarwal, J. Fox, Y. Yun, and M. K. O. Malley, and A. D. Deshpande, "An index finger exoskeleton with series elastic actuation for rehabilitation: Design, control and performance characterization," *Int. J. Robot. Res.*, vol. 34, no. 14, pp. 1747–1772, Dec. 2015.
[56] M. Hara *et al.*, "Design and compatibility of a high-performance actuation system for fMRI-based neuroscience studies," in *Proc. IEEE/RSJ Int. Conf. Intell. Robots Syst. (IROS)*, Oct. 2010, pp. 2437–2442.
[57] R. Xu, A. Yurkewich, and R. V. Patel, "Curvature, torsion, and force sensing in continuum robots using helically wrapped FBG sensors," *IEEE Robot. Autom. Lett.*, vol. 1, no. 2, pp. 1052–1059, Jul. 2016.

Hong Kai Yap (S'15) received the B.Eng. (Hons.) degree in bioengineering from the National University of Singapore (NUS), in 2013. He is currently pursuing the Ph.D. degree at NUS Graduate School for Integrative Sciences and Engineering.

His current research interests include soft robotics, rehabilitation robotics, and MR imaging.

Nazir Kamaldin received the B.Eng. (Hons.) degree in electrical engineering from the National University of Singapore (NUS), in 2013. He is currently pursuing the Ph.D. degree at the NUS Graduate School for Integrative Sciences and Engineering. His current research interests include robust and adaptive control for industrial and medical applications.

Jeong Hoon Lim received the M.D. degree from the College of Medicine, Seoul National University, Seoul, Korea in 1993, the M.S. degree and the Ph.D. degree from Graduate School of Medicine, Seoul National University, Seoul, Korea, in 2002 and 2007, respectively.

He is now a senior consultant at Department of Medicine, National University Hospital and an Assistant Professor at Department of Medicine, Yong Loo Lin School of Medicine, National University of Singapore. His research interest includes spasticity management, neurorehabilitation and rehabilitation robotics.

Fatima A. Nasrallah received the Ph.D. degree in neuroscience from the Department of Medicine, University of New South Wales, Australia, in 2009.

She was a Senior Fellow at the Clinical Imaging Research Center, NUS/A*STAR, Singapore from 2013 to 2015. She is currently a Principal Investigator at the Queensland Brain Institute (QBI), Australia. Her research interest is mainly focused on multimodality imaging and functional MRI.

James Cho Hong Goh received the B.S. degree in mechanical engineering and the Ph.D. degree in bioengineering from University of Strathclyde, Glasgow, U.K., in 1976 and 1982, respectively.

He is currently a Professor and the Head of Department of Biomedical Engineering, National University of Singapore. His research interest includes biomechanics, orthopaedic implants and devices.

Prof Goh is the president of International Federation of Medical and Biological Engineering (IFBME) and Biomedical Engineering Society, Singapore, and a council member of World Council of Biomechanics (WCB) and World Association of Chinese Biomedical Engineers (WACBE).

Chen-Hua Yeow (M'14) received the B.E. degree and the Ph.D. degree in bioengineering from National University of Singapore, Singapore, in 2006 and 2010, respectively. He was a postdoctoral fellow at the BioRobotics Laboratory at Harvard University, Cambridge, MA, USA, from 2010 to 2012.

He is currently an Assistant Professor at the Department of Biomedical Engineering, National University of Singapore, and an affiliated Principal Investigator with Singapore Institute for Neurotechnology and Advanced Robotics Center. His research interest includes surgical and rehabilitation robotics, medical device design, and sports biomechanics.